Electronic Supplementary Information (ESI)

Acetylenedicarboxylate-based cerium(IV) metal-organic framework with fcu net topology: A potential material for air cleaning from toxic halogen vapors

Tobie J. Matemb Ma Ntep,[a] Helge Reinsch,[b] Jun Liang,[a,c] and Christoph Janiak *[a]

[a] Institut für Anorganische Chemie und Strukturchemie, Heinrich-Heine-Universität Düsseldorf, Universitätsstraße 1, D-40225 Düsseldorf, Germany

[b] Institut für Anorganische Chemie, Christian-Albrechts-Universität, Max-Eyth-Straße 2, 24118 Kiel, Germany

[c] Hoffmann Institute of Advanced Materials, Shenzhen Polytechnic, 7098 Liuxian Blvd, Nanshan District, Shenzhen 518055, China

* Corresponding author: E-mail: janiak@uni-duesseldorf.de; Fax: + 49-211-81-12287; Tel: +49-211-81-12286
Additional email addresses:
tobie.matemb.ma.ntep@uni-duesseldorf.de; hreinsch@ac.uni-kiel.de; liangj@hhu.de

Table of contents

Comparison of simulated PXRD patterns of fcu cerium acetylenedicarboxylate MOF Ce-HHU-1 and zirconium acetylenedicarboxylate Zr-HHU-1

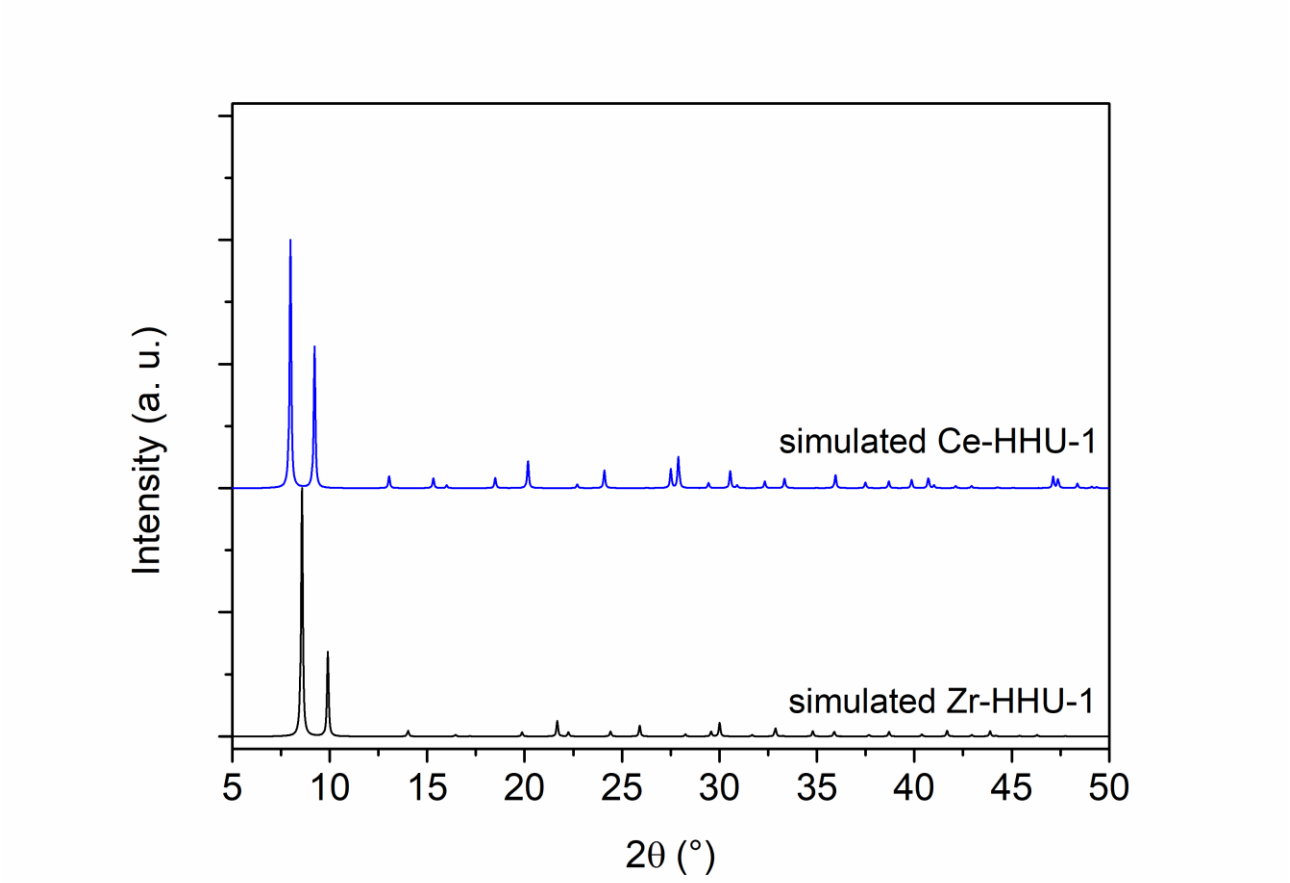

Fig. S1 Simulated PXRD pattern of Ce-HHU-1 in comparison with the simulated PXRD pattern of Zr-HHU-1.

Infrared and Raman spectroscopy of fcu cerium acetylenedicarboxylate MOF Ce-HHU-1

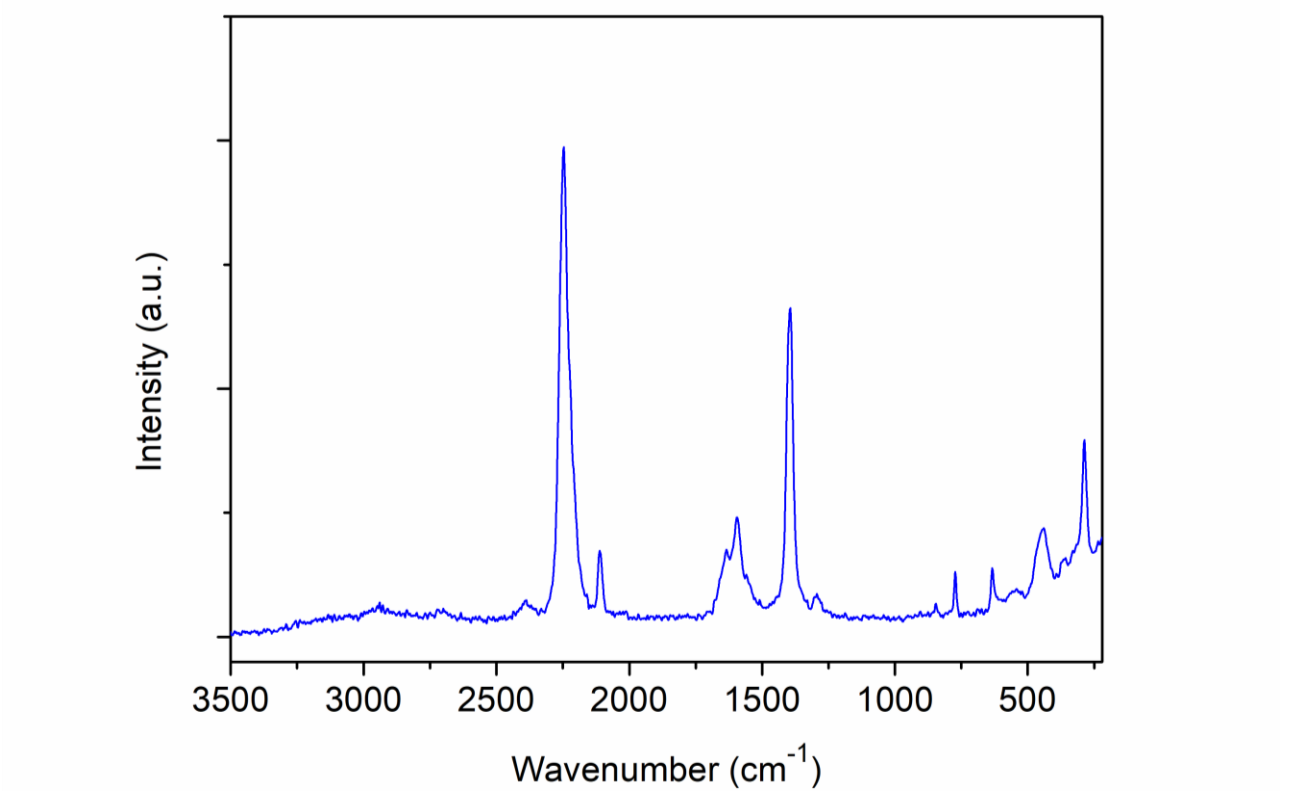

Fig. S2 Raman spectrum of Ce-HHU-1. The strong band at 2225 cm^{-1} is ascribed to the vibration of the C≡C triple-bond of acetylenedicarboxylate.

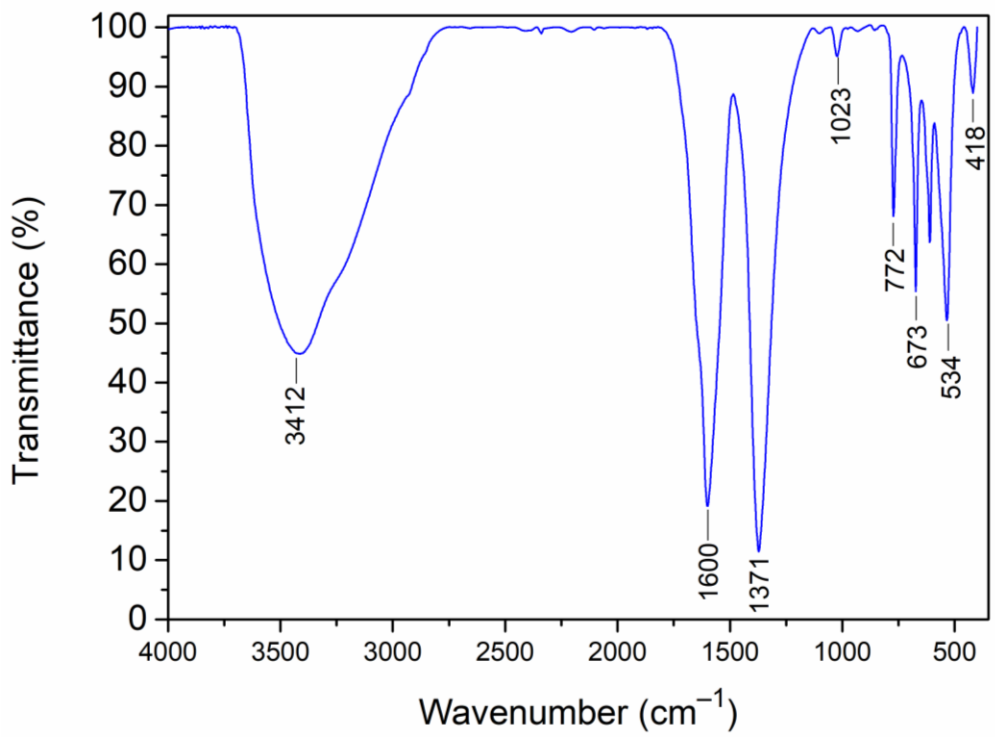

Fig. S3 Infrared spectrum of cerium(IV) acetylenedicarboxylate MOF Ce-HHU-1.

Thermogravimetric analysis of Ce-HHU-1 with missing linker defect calculation

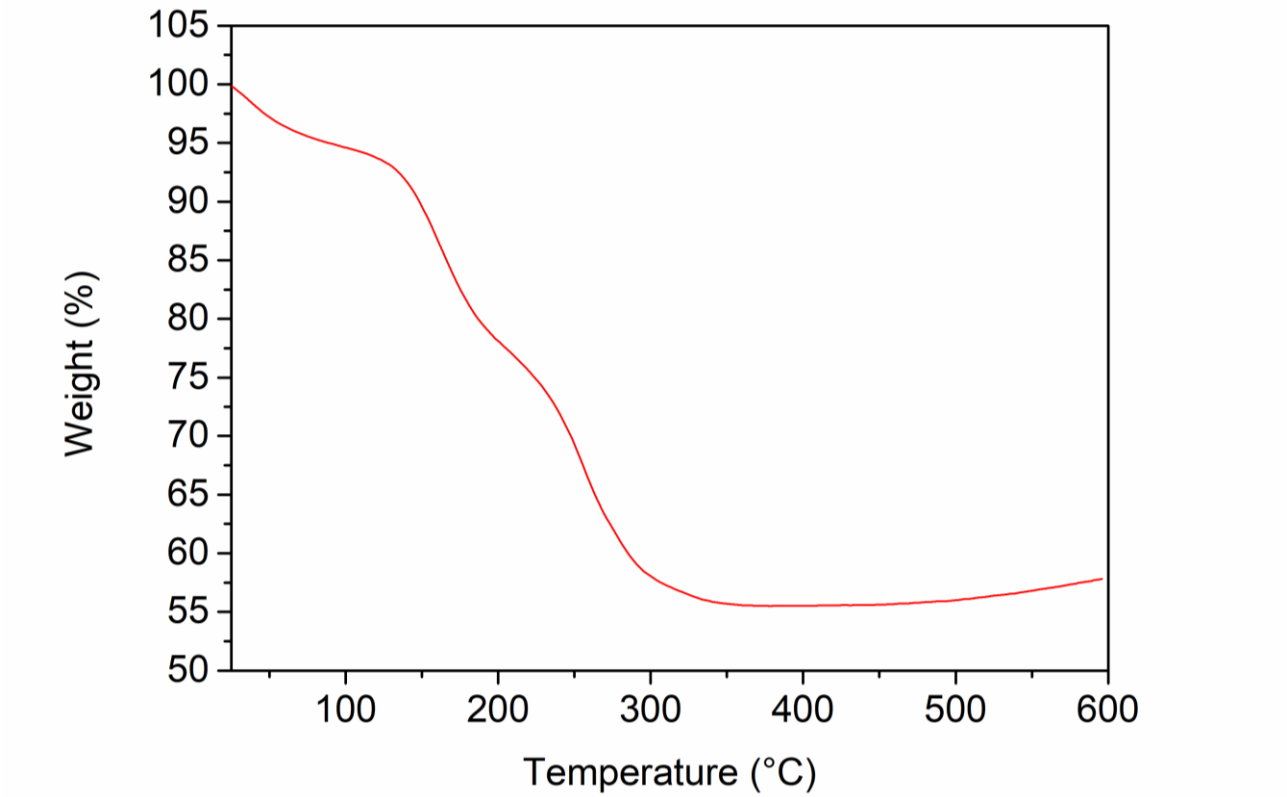

Fig. S4 Trace of the thermogravimetric analysis under air at a heating rate of 5 K min^{-1} for Ce-HHU-1. The slight rise of the TGA curve in the temperature range 500-600 °C is a measurement artifact, which we frequently observe with our Netzsch TGA. The origin of this artifact could not be elucidated. Hence, this rise should not be given a particular attention. A possibility could be the instability of the thermobalance in this temperature range during the measurement. Further, the rise of the TGA curve happened after complete decomposition of Ce-HHU-1 and has therefore no effect on the thermogram profile of Ce-HHU-1. The more so, as the final solid residue was identified as CeO_2 which is expected already at 350 °C, in agreement with the thermal decomposition profile of for example Ce-UiO-66 and Ce-Fum.[1]

- Missing linker defect calculation (according to Shearer *et al.*[2])

The ideal (defect-free) Ce-HHU-1 (Ce-ADC) MOF formula is $[Ce_6O_4(OH)_4(ADC)_6]$.

The complete decomposition of ideal Ce-HHU-1 would yield $6CeO_2$ solid residue.

Mass of solid residue: $6 \times M(CeO_2) = 1032.66$ g mol^{-1}

Molar mass of ideal Ce-HHU-1: $M[Ce_6O_6(ADC)_6] = 1644.97$ g mol^{-1}, a factor of 1.5929 higher than the solid residue.

The ideal plateau of MOF should then be found at 159.3% on the TG trace normalized to 100% solid residue i.e $Wt_{ideal\ plat.} = 159.3\%$ and $W_{end} = 100\%$ (see Fig. S4b).

The experimental plateau of the TG curve is found at $Wt_{exp.plat.} \approx 161\%$.

A value for expected weight loss per ADC linker out of $NL_{ideal} = 6$ linkers is:

$Wt_{pL.teo} = (Wt_{ideal\ plat.} - W_{end}) / NL_{ideal} = (159.29 - 100) / 6 = 9.88\%$

The number of experimental linkers per Ce_6 cluster is:

$NL_{exp.} = 6 - x = (Wt_{exp.\ plat.} - W_{end}) / Wt_{pL.theo} = (160.8 - 100) / 9.88 = 6.15 \approx 6$ which implies no occurrence of missing linker defects in the framework of Ce-HHU-1 obtained. This conclusion is in agreement with the result of the CHN elemental analysis.

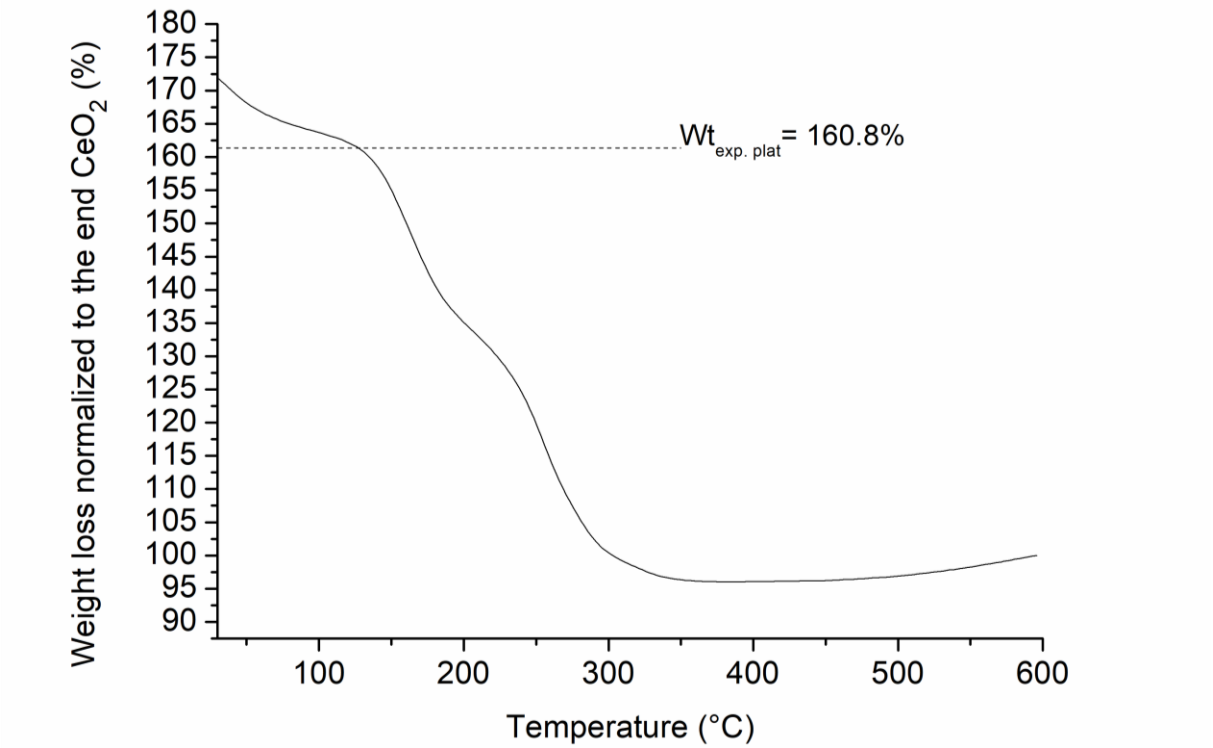

Fig. S4b Normalized TGA curve of Ce-HHU-1.

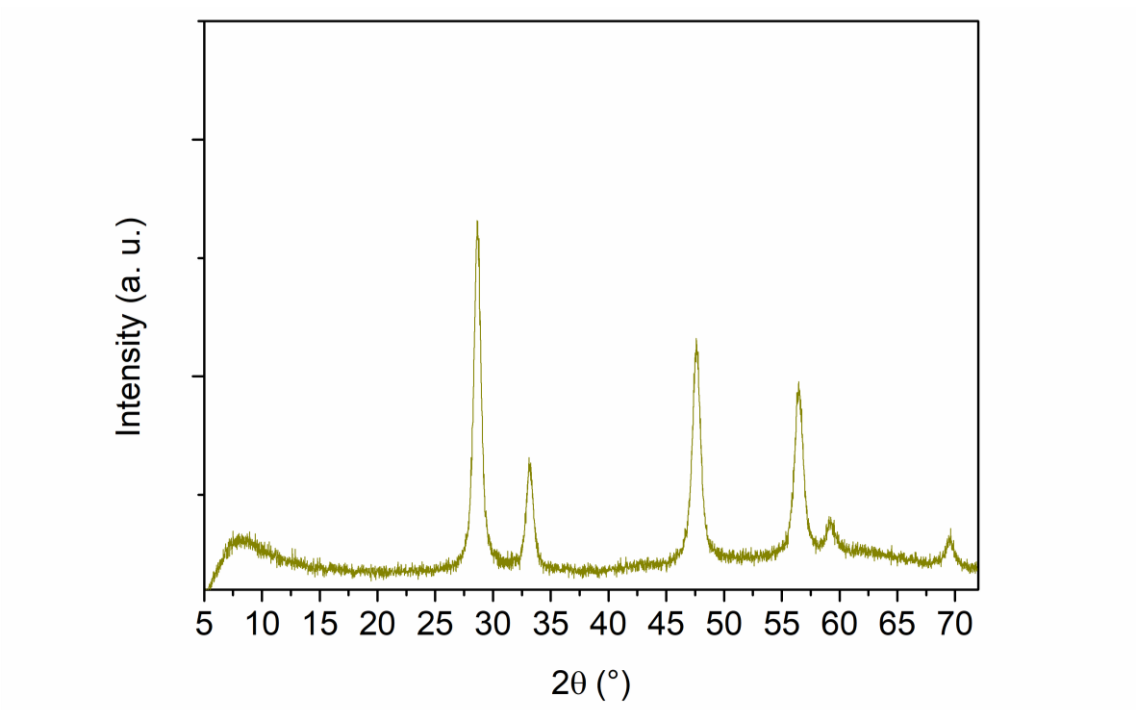

Fig. S5 PXRD pattern of the solid residue after TGA analysis. The pattern corresponds to the cubic fluorite-type phase of CeO_2.[3]

PXRD patterns of the chemical stability test for Ce-HHU-1

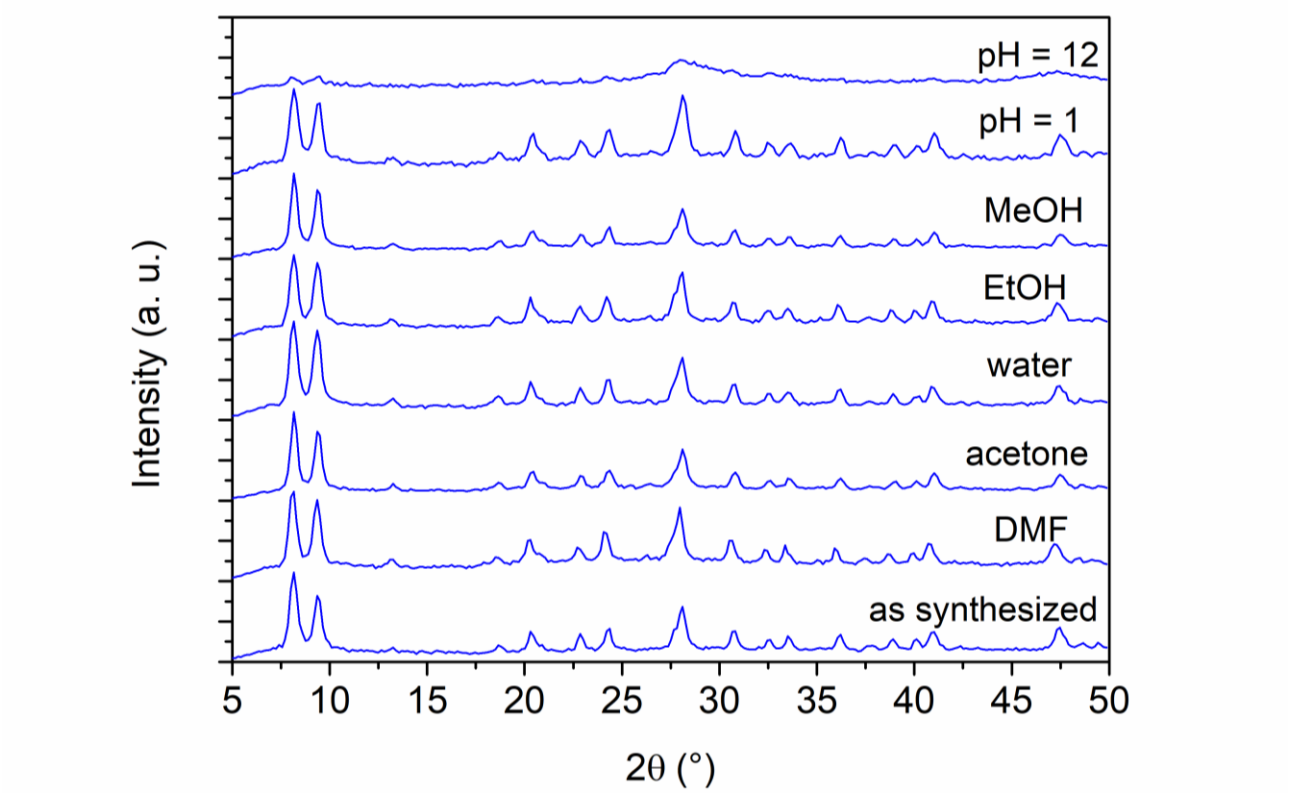

Fig. S6 PXRD patterns of Ce-HHU-1 after stirring 24 h at room temperature in various solvents and solutions (top). PXRD of Ce-HHU-1 after water sorption experiment (bottom).

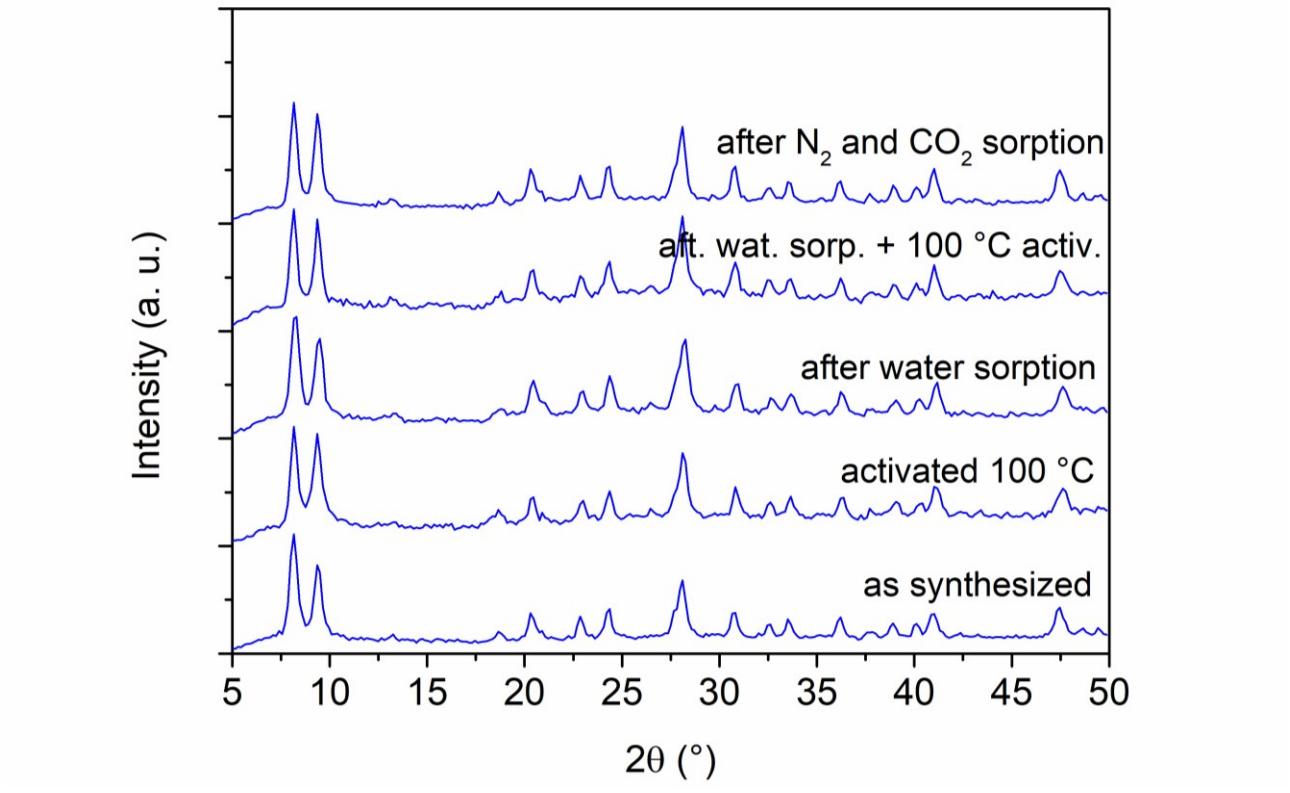

Fig. S7 PXRD patterns of Ce-HHU-1 after activation at 100 °C, after water and gas sorption.

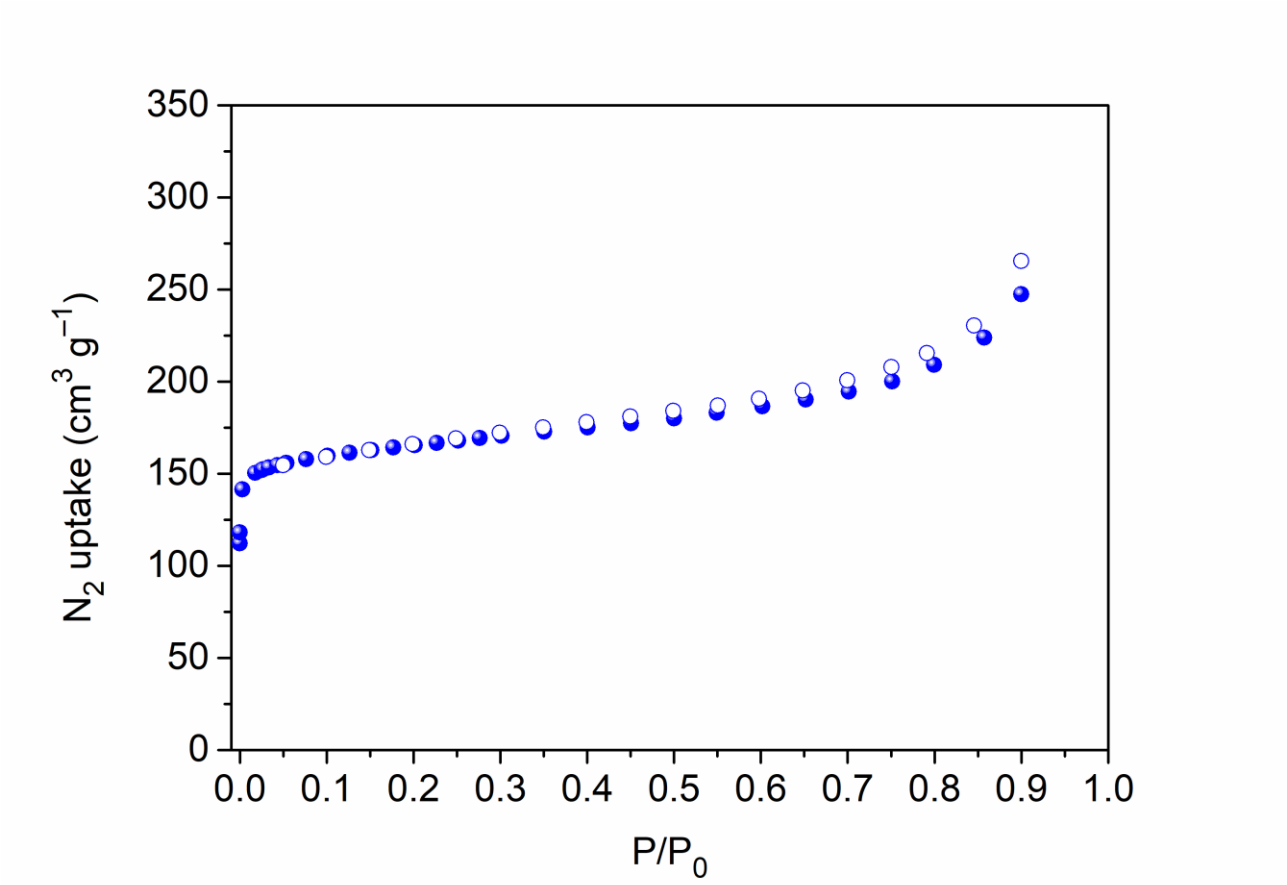

Fig. S8 Nitrogen sorption isotherm of Ce-HHU-1 after water sorption, followed by activation at 100 °C under vacuum.

Method of structure determination by Rietveld refinement for Ce-HHU-1

For the refinement of Ce-HHU-1 structure, the crystal structure of Hf-HHU-1 was used as starting model for the Rietveld refinement after exchanging the Hf atoms for Ce atoms and superimposing the cell parameter deduced from the position of the second peak (hkl = 200). All atoms were freely refined using one temperature factor for the framework and one temperature factor for the guest atoms, respectively. The occupancy of the linker molecules was also freely refined. Residual electron density inside the pores was identified by Fourier synthesis and attributed to guest molecules, modeled by oxygen atoms of refinable occupancy. These guest atoms (G*n*) should be considered placeholders for any kind of solvent molecules. The linker occupancy converged to ≈ 0.69. It must be mentioned that the modeling of the guest atoms could easily affect this and thus this value should be carefully interpreted. Some relevant parameters are summarized in Tab. 1 and the final plot is shown in Fig. 2. Crystallographic data for the structural analyses of Ce-HHU-1 have been deposited with the Cambridge Crystallographic Data Centre (CCDC 1946853).

Tab. S1 Summary of some reported CO_2 uptake capacity of Ce(IV)-based MOFs .

Materials	S_{BET} ($m^2\ g^{-1}$)	CO_2 uptake (mmol g^{-1}, 273 K)	CO_2 uptake (mmol g^{-1}, 293 K)	Structure	Ref
Ce-HHU-1	793	3.2	2.5	fcu	This work
Ce-UiO-66-$(CH_3)_2$	845	1.5	1.0	fcu	4
F_4_UiO-66(Ce)	641	2.5	1.5	fcu	5
F_4_MIL-140A(Ce)	320	2.1	1.9	MIL-140	2
Ce-UiO-66-N_3	835	2.6	–	fcu	6
Ce-UiO-66-NO_2	819	3.7	–	fcu	3
Ce-CCA	1210	1.6	–	fcu	7

CCA = 4-carboxycinnamate

Bromine adsorption for Ce-HHU-1

Fig. S9 Photograph of the product obtained after bromine vapour adsorption on Ce-HHU-1.

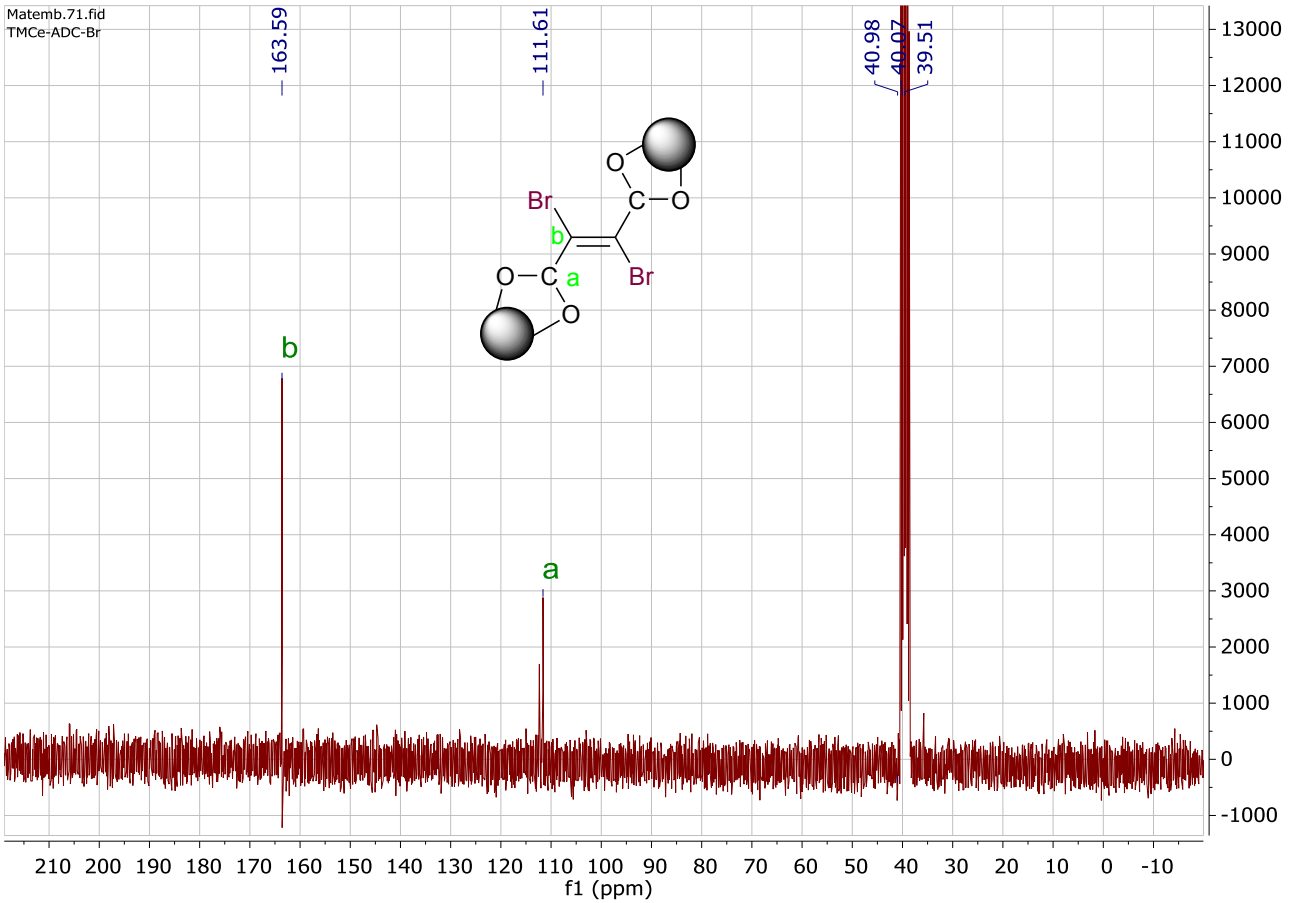

Fig. S10 Liquid ^{13}C NMR spectrum of product obtained after bromine vapor adsorption onto Ce-HHU-1 (Ce-HHU-1-Br_2).

Iodine adsorption for Ce-HHU-1

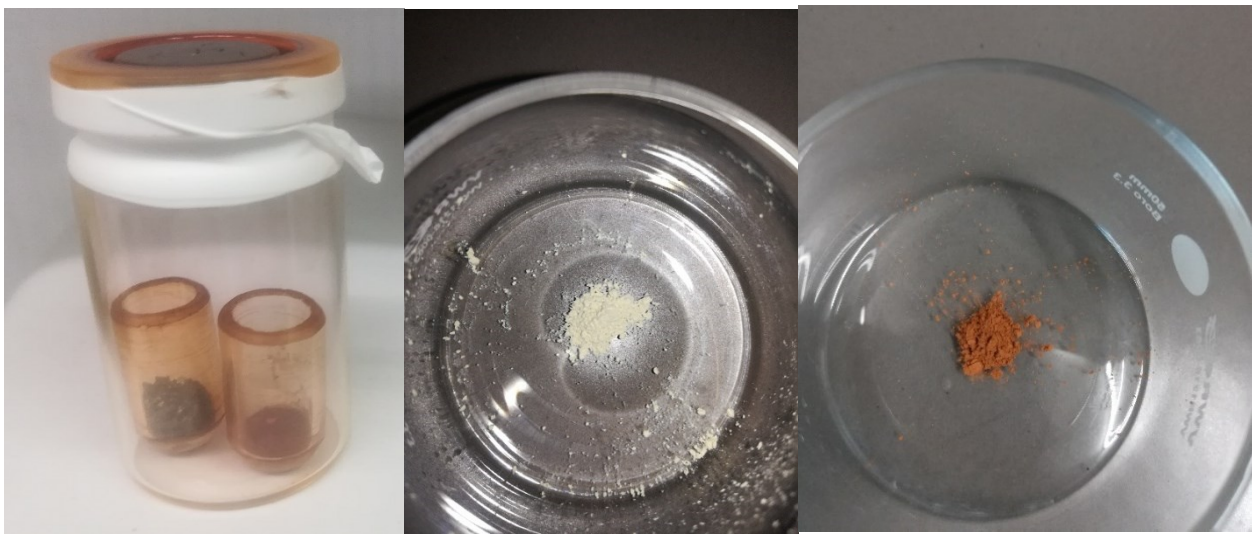

Fig. S11 Photographs of the set up for iodine adsorption (left), Ce-HHU-1 before iodine adsorption (middle) and after iodine loading (right).

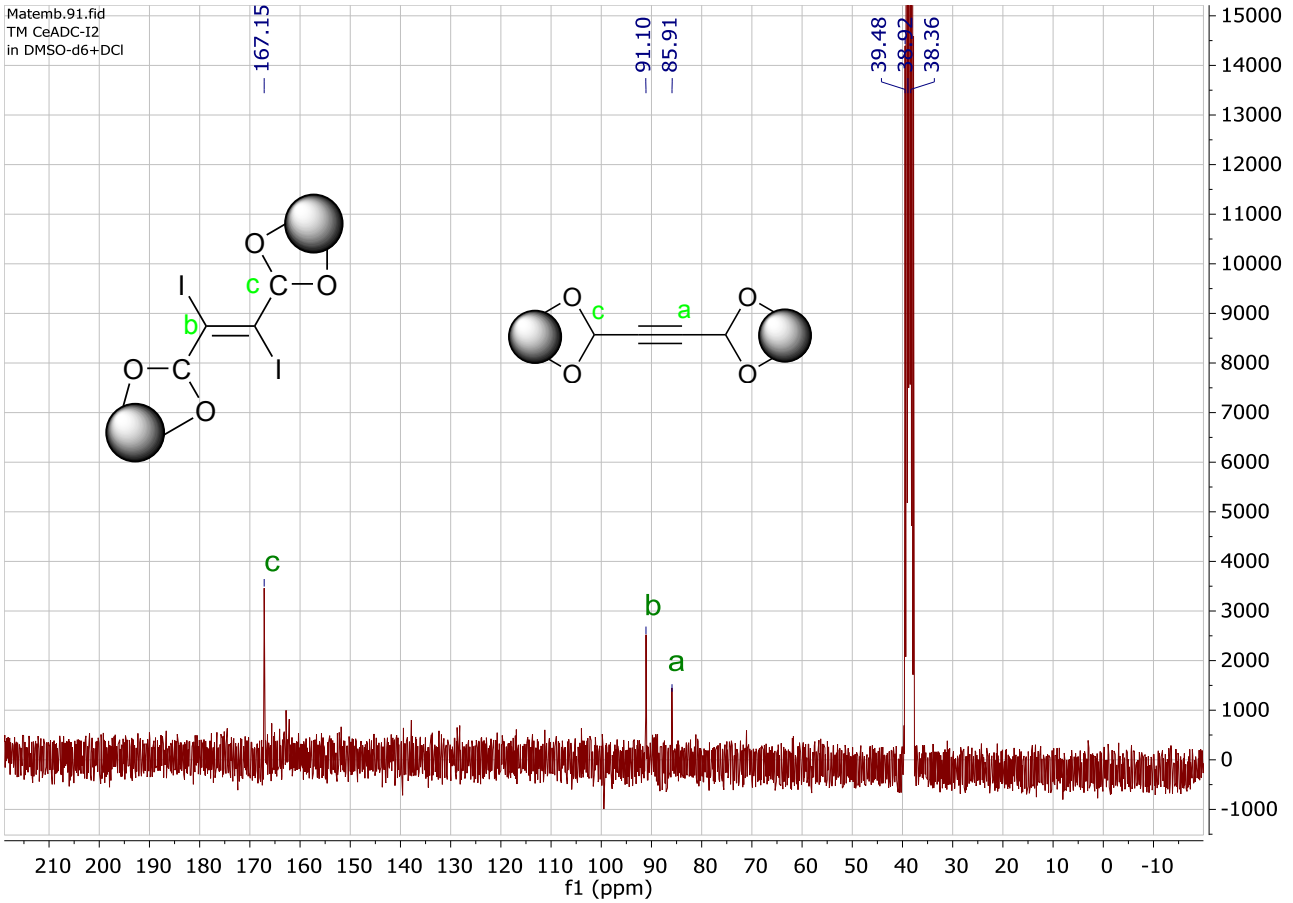

Fig. S12 Liquid ^{13}C NMR spectrum of Ce-HHU-1-I_2 after iodine desorption (washing) in ethanol over a week to a colorless supernatant washing solvent.

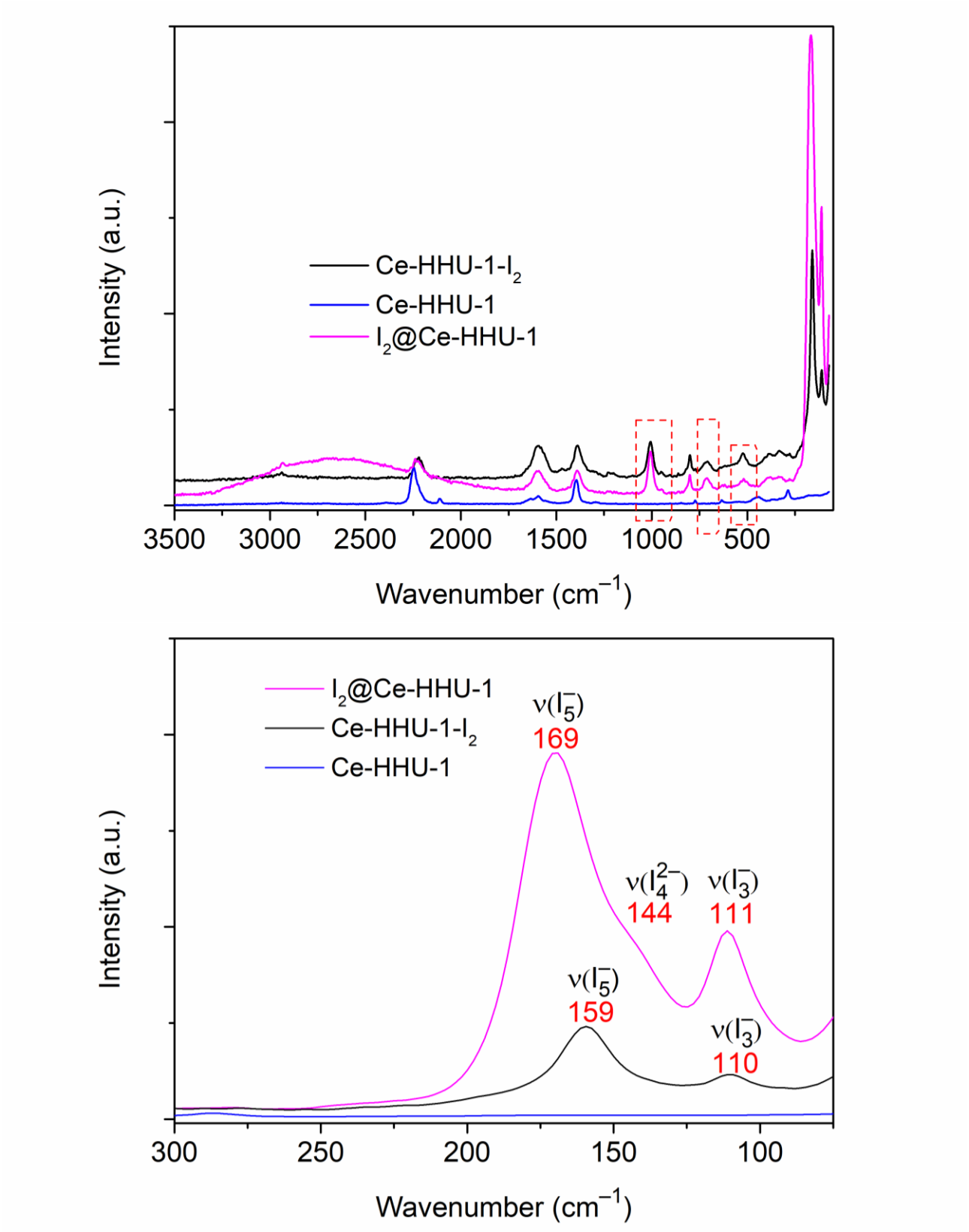

Fig. S13 Raman spectra of activated Ce-HHU-1 (blue), iodine-loaded I_2-Ce-HHU-1 (pink) and desorbed/ethanol washed Ce-HHU-1-I_2. Spectra in the 3500-50 cm^{-1} range (top) and in the 300-50 range (bottom).

Determination of the isosteric heat of CO_2 adsorption

The CO_2 isotherms experimentally obtained respectively at 273 K and 298 K were fitted with the Langmuir-Freundlich model (eq. 1). The fits are shown in Figure S14. The obtained fits were used to determine the pressure for each temperature corresponding to various CO_2 loadings. The isosteric heat of adsorption was finally calculated by applying the Clausius-Clapeyron equation (eq. 2).

$$q = q_{max} \cdot \frac{(k \cdot p)^t}{1 + (k \cdot p)^t} \qquad (1)$$

q is the gas amount adsorbed (mmol g^{-1}); q_{max} is the maximum loading; k is the affinity constant (bar^{-1}); t is the heterogeneity exponent; p is the pressure (kPa).

$$Q_{st} = -R\left(\frac{T_2 T_1}{T_2 - T_1}\right) ln \frac{P_2}{P_1} \qquad (2)$$

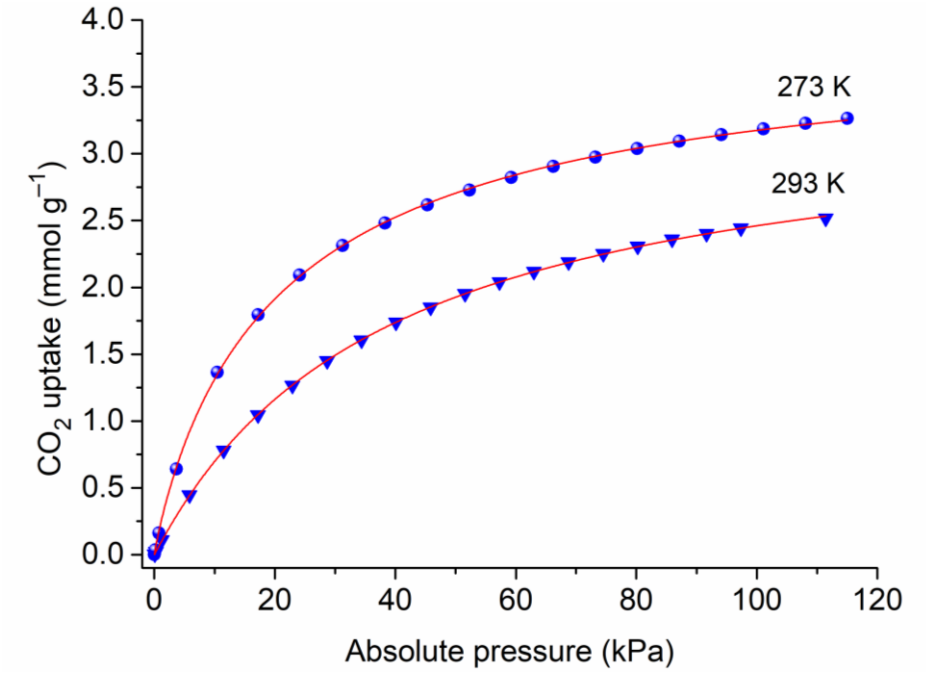

Fig. S14 Fitting of CO_2 adsorption isotherms with the Langmuir-Freundlich model. Symbols for experimental data and red lines for simulated fits.

Scanning electron microscopy (SEM)

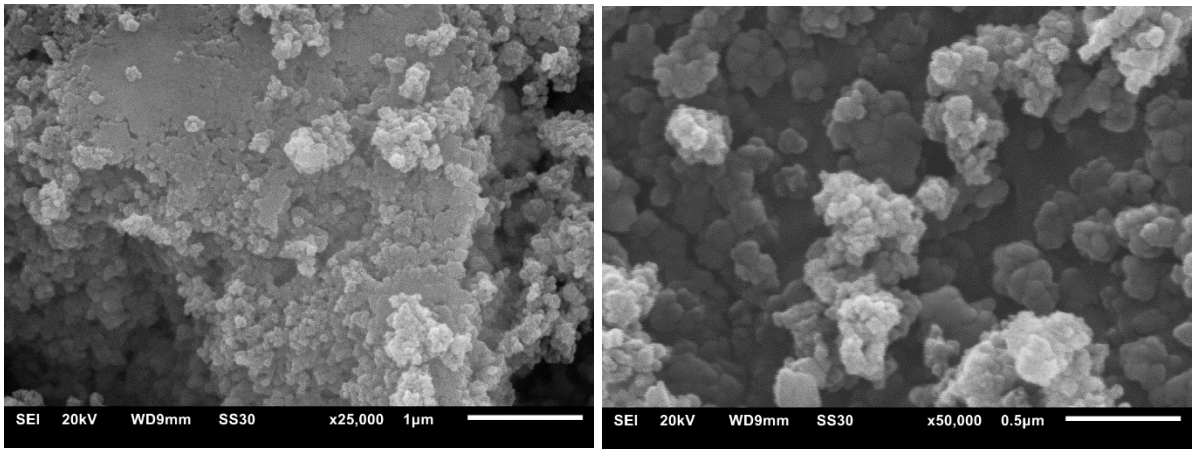

Fig. S15 Scanning electron micrographs (SEM) of Ce-HHU-1.

REFERENCES

1 M. Lammert, M. T. Wharmby, S. Smolders, B. Bueken, A. Lieb, K. A. Lomachenko, D. De Vos and N. Stock, *Chem. Commun.*, 2015, **51**, 12578–12581.
2 G. C. Shearer, S. Chavan, S. Bordiga, S. Svelle, U. Olsbye and K. P. Lillerud, *Chem. Mater.*, 2016, **28**, 3749-3761.
3 L. Zhang, W. Zou, K. Ma, Y. Cao, Y. Xiong, S. Wu, C. Tang, F. Gao and L. Dong, *J. Phys. Chem. C*, 2015, **119**, 1155−1163.
4 R. Dalapati, B. Sakthivel, A. Dhakshinamoorthy, A. Buragohain, A. Bhunia, C. Janiak and S. Biswas, *CrystEngComm*, 2016, **18**, 7855–7864.
5 R. D'Amato, A. Donnadio, M. Carta, C. Sangregorio, D. Tiana, R. Vivani, M. Taddei and F. Costantino, *ACS Sustainable Chem. Eng.*, 2019, **7**, 394−402.
6 A. Buragohain and S. Biswas, *CrystEngComm*, 2016, **18**, 4374–4381.
7 M. SK, M. Grzywa, D. Volkmer and S. Biswas, *Microporous Mesoporous Mat.*, 2017, **237**, 275–281.